Structural Engineering and Mechanics, *Vol. 67, No. 5 (2018) 505-516*
DOI: https://doi.org/10.12989/sem.2018.67.5.505

Investigation of the effects of particle size and model scale on the UCS and shear strength of concrete using PFC2D

Hadi Haeri*[1], Vahab Sarfarazi[2a], Zheming Zhu**[1] and Hossein Ali Lazemi[3]

[1]*College of Architecture and Environment, Sichuan University, Chengdu 610065, China*
[2]*Department of Mining Engineering, Hamedan University of Technology, Hamedan, Iran*
[3]*Department of Mining Engineering, Bafgh Branch, Islamic Azad University, Bafgh, Iran*

(Received April 4, 2018, Revised June 3, 2018, Accepted June 7, 2018)

Abstract. In this paper, the effects of particle size and model scale of concrete has been investigated on the failure mechanism of PFC2D numerical models under uniaxial compressive test. For this purpose, rectangular models with same particle sizes and different model dimensions, i.e., 3 mm×6 mm, 6 mm×12 mm, 12 mm×24 mm, 25 mm×50 mm and 54 mm×108 mm, were prepared. Also rectangular models with dimension of 54 mm×108 mm and different particle sizes, i.e., 0.27 mm, 0.47 mm, 0.67 mm, 0.87 mm, 1.07 mm, 1.87 mm and 2.27 mm were simulated using PFC2D and tested under uniaxial compressive test. Concurrent with uniaxial test, direct shear test was performed on the numerical models. Dimension of the models were 75×100 mm. Two narrow bands of particles with dimension of 37.5 mm × 20 mm were removed from upper and lower of the model to supply the shear test condition. The particle sizes in the models were 0.47 mm, 0.57 mm, 0.67 mm and 0.77 mm. The result shows that failure pattern was affected by model scale and particle size. The uniaxial compressive strength and shear strength were increased by increasing the model scale and particle size.

Keywords: model scale; particle size; uniaxial compression test; direct shear test; PFC2D

1. Introduction

Concrete is currently the most widely used construction material in the world. In fact, an average of about one (1) cubic meter of concrete per capita is produced annually. The design of concrete structures requires a thorough understanding of their material properties under various loading condition. Several experimental investigations have been carried out to examine the behavior of concrete (Shuraim 2016, Haeri *et al*. 2016, Shaowei *et al*. 2016). The correlation between the strength of concrete and their geometrical dimensions is known as the size effect. The size effects introduce a challenge to the transference of small-scale measured strength data to the large-scale structures. to investigate the size effect on strength and fracture energy of concrete, with the experimental results well documented in several published papers such as in Van Vliet (2000) and further analyzed by other researchers such as Vorechovsky (2007). Van Vliet (2000) conducted a series of uniaxial tension experiments using dog bone shaped specimens. Zi *et al.* (2014) studied the size effect on equi-biaxial flexure strength of concrete by the ASTM C1550 flexure test and the ring-on-ring flexure of circular plates. The four-point flexure test of prismatic beams was also carried out to obtain uniaxial flexural strength for comparison. These researches exhibit scale dependency in terms of tensile strength, due to the differences in micro-defects and macroscopic cracks. This important may be occurs in distinct element simulation. The distinct element method (DEM) allows fracturing and differential displacements between individual elements. PFC2D, a special DEM code, is based on circular elements and the fundamental laws of contact physics (Cundall 1971, Cundall and Strack 1979, Itasca 1999). Thus, it is ideal to simulate the behaviour of granular materials such as rock. PFC2D elements can also be bonded to describe consolidated rock and, in turn, bond breakage can be used to study fracture mechanics. The PFC codes have been applied for solving many rock mechanics problems at laboratory scales, such as tri-axial testing of rocks with complete stress–strain curves (Aoki 2004), failure around a circular opening under bi-axial compression (Fakhimi 2002), direct shear test of a rock fracture (Cundall 2001, Sarfarazi 2016, Haeri 2016), acoustic emissions (AE) (Hazzard 2000, 2004) and hydro-fracturing tests of granite (Al-Busaidi) for laboratory scale simulations. Also PFC has been used to simulate large field scale rock engineering problems such as tunnel/ cavern excavation and evaluation of EDZ (Aoki 2004), tunnel face stability (Okabe 2004), design of tunnel lining (Tannant 2004), rock cutting and slope stability analysis (Wang 2003), mining (e.g., Sainsbury *et al.* 2003, Diederichs *et al.* 2004), rock mechanics (e.g., Holt *et al.* 2003) and slope stability (e.g., Wang *et al.* 2003), sliding friction and the formation of fault gouges (e.g. Mora and Place 1998, Morgan and Boettcher 1999), seismic events and the short-time response of adjacent rocks (Mora and Place 1993, Scott 1996, Dalguer *et al.* 2003), large-scale kinematics of

*Corresponding author, Assistant Professor
E-mail: haerihadi@gmail.com
**Corresponding author, Professor
E-mail: zhemingzhu@hotmail.com
[a]Assistant Professor

ISSN: 1225-4568 (Print), 1598-6217 (Online)

geodynamic processes (Erickson *et al.* 2001, Burbidge and Braun 2002, Strayer and Suppe 2002, Vietor 2003, Zhou *et al.* 2016, Zhou *et al.* 2018, Zhou *et al.* 2016, Wang *et al.* 2018, Wang *et al.* 2018, Wang *et al.* 2018), rock mass with non-persistent joints (Bahaaddini *et al.* 2013b, Fan *et al.* 2015, Ghazvinian *et al.* 2012, Park *et al.* 2004, Scholtès and Donzé 2012), especially with the development of smooth joint contact model (Hadjigeorgiou *et al.* 2009, Esmaieli *et al.* 2010, Mas Ivars *et al.* 2011, Chiu *et al.* 2013, Bahaaddini *et al*. 2013a, 2013b, 2014, Lambert and Coll 2014). Many researchers have been accomplished to study the cracks initiation, propagation and coalescence in the cracked specimens containing a few open flaws under uniaxial, biaxial and shear loading (Zhou and Yang 2007, Zhou 2010, Lancaster *et al.* 2013, Zhou and Yang 2012, Mobasher *et al.* 2014, Noel and Soudki 2014, Oliveira and Leonel 2014, Kim and Taha 2014, Tiang *et al.* 2015, Wan Ibrahim *et al.* 2015, Silva *et al.* 2015, Liu *et al.* 2015, Haeri 2015, Haeri *et al.* 2015a, b, Haeri *et al.* 2016, Fan *et al.* 2016, Li *et al.* 2016, Sardemir 2016, Sarfarazi *et al.* 2016, Shuraim 2016, Wang *et al.* 2016, 2017, Zhou and Wang 2016, Shemirani *et al.* 2016, Sarfarazi *et al.* 2017a, b, c, Wang *et al.* 2017, Shemirani *et al.* 2018, Zhou and Bi 2018a, b, Haeri *et al*. 2013, Haeri *et al*. 2014, Haeri 2015, Haeri and Sarfarazi 2016a, b; Haeri *et al*. 2016).

In previous research, the effects of model scale and particle size on engineering problem were ambiguous. Investigations of the effects of model scale and particle size on tensile strength, point load index and failure processes of numerical models is important to justify the applicability of the numerical modeling results. PFC2D numerical model has advantages in simulation failure mechanism under uniaxial compressive test over than other numerical methods such as crack initiation stress, crack propagation and crack coalescence. In this paper, various models with different scales and different particle sizes were simulate using PFC2D and tested under both of the compression test and shear test. The effects of model scale and particle size were cleared on the failure pattern of models, compressive strength and shear strength.

2. General features of PFC2D

A two dimensional distinct element method is used in form of computer code known as particle flow code (PFC2D) to numerically simulate the laboratory specimens (Itasca 1999 version 3.1; Potyondy and Cundall 2004). This distinct element code represents the material specimen as an assembly of rigid particles so that each particle can move independently and may interact with other particles at contact points. A central finite difference scheme is adopted in the discrete element method (DEM) to calculate the movements and interaction forces of these particles. In this approach two contact models are usually in use i.e., the linear and non-linear contact models. In this study the linear contact model is preferred which provides a linear elastic relation in between the displacements and contact forces of the particles within the particle assembly. Fig. 6 shows the basic linear contact model adopted in in the PFC code which is known as the contact force–displacement relationship. In this model, the linear point contact in between each two particles of the assembly is shown which relating the contact normal force component, F^n, contact overlap, U^n, increment of shear force, ΔF^s, and shear displacements, ΔU^s as given in the following equations.

$$\left\{ \begin{array}{c} F^n = K^n U^n \\ \Delta F^s = -k^s \Delta U^s \end{array} \right\} \tag{1}$$

where K^n and k^s are the normal and shear stiffness of the contact, respectively. The frictional strength of the contact can be expressed as

$$F^s \leq \mu F^n \tag{2}$$

where μ is the coefficient of friction in between the particles. The relative movements in between the individual particles within the particle assembly can only be represented by Eq. (1). As a whole, when a group of bounded particles are to be considered in form of an assembly, the cemented contacts including both contact forces and torques are needed as shown in Figs. 6(a) and 6(c). Therefore, the relationships between these incremental quantities can be formulated as

$$\left\{ \begin{array}{c} \Delta \bar{F}^n = \bar{k}^n A \Delta U^n \\ \Delta \bar{F}^s = -\bar{k}^s A \Delta U^s \end{array} \right\} \quad \left\{ \begin{array}{c} \Delta \bar{F}^n = \bar{k}^n A \Delta U^n \\ \Delta \bar{F}^s = -\bar{k}^s A \Delta U^s \end{array} \right\} \tag{3}$$

which are the incremental force-displacement relations and the incremental contact moments are expressed as

$$\left\{ \begin{array}{c} \Delta \bar{M}^n = -\bar{k}^s J \Delta \theta^n \\ \Delta \bar{M}^s = -\bar{k}^n I \Delta \theta^s \end{array} \right\} \tag{4}$$

where F^n, F^s; M^n and M^s are the force components and torques (moments) about the center of the cemented-contact zone, respectively. k^n and k^s represent the normal and shear bond stiffness per unit area, θ^n and θ^s are the components of rotation angle, and A, I, and J are the area, moment of inertia, and polar moment of inertia of the bond cross-section, respectively. Then, the strength of the cemented contact can be written as

$$\begin{gathered} \bar{\sigma}^{max} = \frac{-\bar{F}^n}{A} + \frac{|\bar{M}^s|\bar{R}}{I} < \bar{\sigma}_c \\ \bar{\tau}^{max} = \frac{-\bar{F}^s}{A} + \frac{|\bar{M}^n|\bar{R}}{J} < \bar{\tau}_c \end{gathered} \tag{5}$$

where R is the radius of the cemented zone as depicted in Fig. 6(c), the stresses σ_c and τ_c are the tensile and shear strength of the cemented contact, respectively. However, the contact and bond stiffness can be used to relate the Young's modulus for particle contacts E_c and particle bondage $\bar{E}_c$ as

$$\begin{gathered} E_c = \frac{k_n}{2t} \ (t = 1 \text{ in 2D}) \\ \bar{E}_c = \bar{k}_n (R^{(A)} + R^{(B)}) \end{gathered} \tag{6}$$

where $R^{(A)}$ and $R^{(B)}$ are the radii of two circular particles in contact (Figs. 6(b), (c)). The cemented contacts expressed in Eqs. (3) to (8) are termed as parallel bonds in the PFC

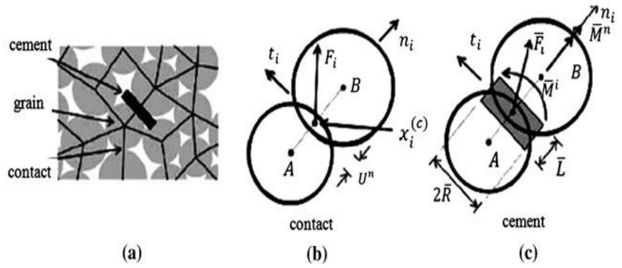

Fig. 6 The force-displacement relationships for the bonding particle system (Potyondy and Cundall 2004)

code. The mechanical properties of rock like materials can be simulated by using the parallel bond model (e.g., Peshkin and Sanderson 1989).

A parallel-bonded model can be generated for PFC2D by using the suitable routines provide by Itasca (1999); version 3.1. however, some of the main micro-properties that should be defined may include: the ball-to-ball contact modulus, the stiffness ratio kn over ks, the friction coefficient of the ball, the normal and shear strengths of the bond, the ratio of standard deviation to the mean of both normal and shear strengths of the bond, the minimum Ball radius, the parallel-bond radius multiplier, the parallel-bond modulus, and the parallel-bond stiffness ratio. A calibration procedure is conducted to provide the appropriate micro properties to be used for the particle assembly. It is not possible to directly determine the particle contact properties and bonding characteristics of the particle assembly from the laboratory tests performed on laboratory model samples. The continuum behavior of the experimentally tested samples can be depicted from the macro-mechanical properties measured by these tests but the appropriate micro-mechanical properties for the numerically simulated modelled specimens can also be gained by using these testing results. Therefore, an inverse modeling procedure based on the trial and error approach is adopted to determine the appropriate micro-mechanical properties of the numerical models from the macro-mechanical properties determined in the laboratory tests (Itasca 1999). In this approach it is assumed some micro-mechanical property values and then solves the problem based on these assumed values. In the second stage the numerically estimated strength and deformation characteristics of the particle assembly are compared with those of the laboratory samples. This procedure is repeated till the micro-mechanical property values that give a simulated macroscopic response close to those measured from laboratory tests. These adjusted values of the micro-mechanical properties are then adopted for the mechanical analyses of discontinuous jointed blocks (Seyferth 2006).

3. Preparing and calibrating the numerical model

The standard process of generation of a PFC2D assembly to represent a test model involves four steps: (a) particle generation and packing the particles, (b) isotropic stress installation, (c) floating particle elimination, and (d) bond installation.

Table 1 Micro properties used to represent the model with tensile strength of 3.6 MPa

Property	Value	Property	Value
Type	Disc	Parallel bond radius multiplier	1.4
Density (kg/m^3)	3000	Young's modulus of parallel bond (GPa)	1.7
Minimum radius (mm)	0.27	Parallel bond stiffness ratio (pb_kn/pb_ks)	3
Size ratio	1.56	Particle friction coefficient	0.5
Porosity ratio	0.05	Parallel normal strength, mean (MPa)	50
Local damping coefficient	0.7	Parallel normal strength, std. dev (MPa)	5
Contact young modulus (GPa)	12	Parallel shear strength, mean (MPa)	50
Stiffness ratio (kn/ks)	1.7	Parallel shear strength, std. dev (MPa)	5

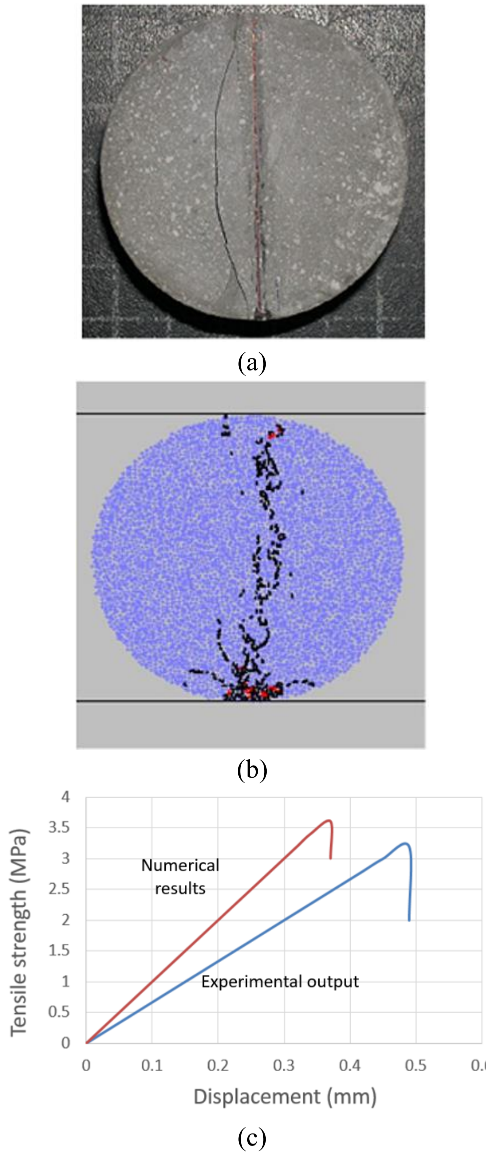

Fig. 1(a) failure pattern in (a) physical sample, (b) PFC2D model. (c) numerical tensile strength and a comparison of its experimental measurements

3.1 Brazilian test

Brazilian test was used to calibrate the tensile strength

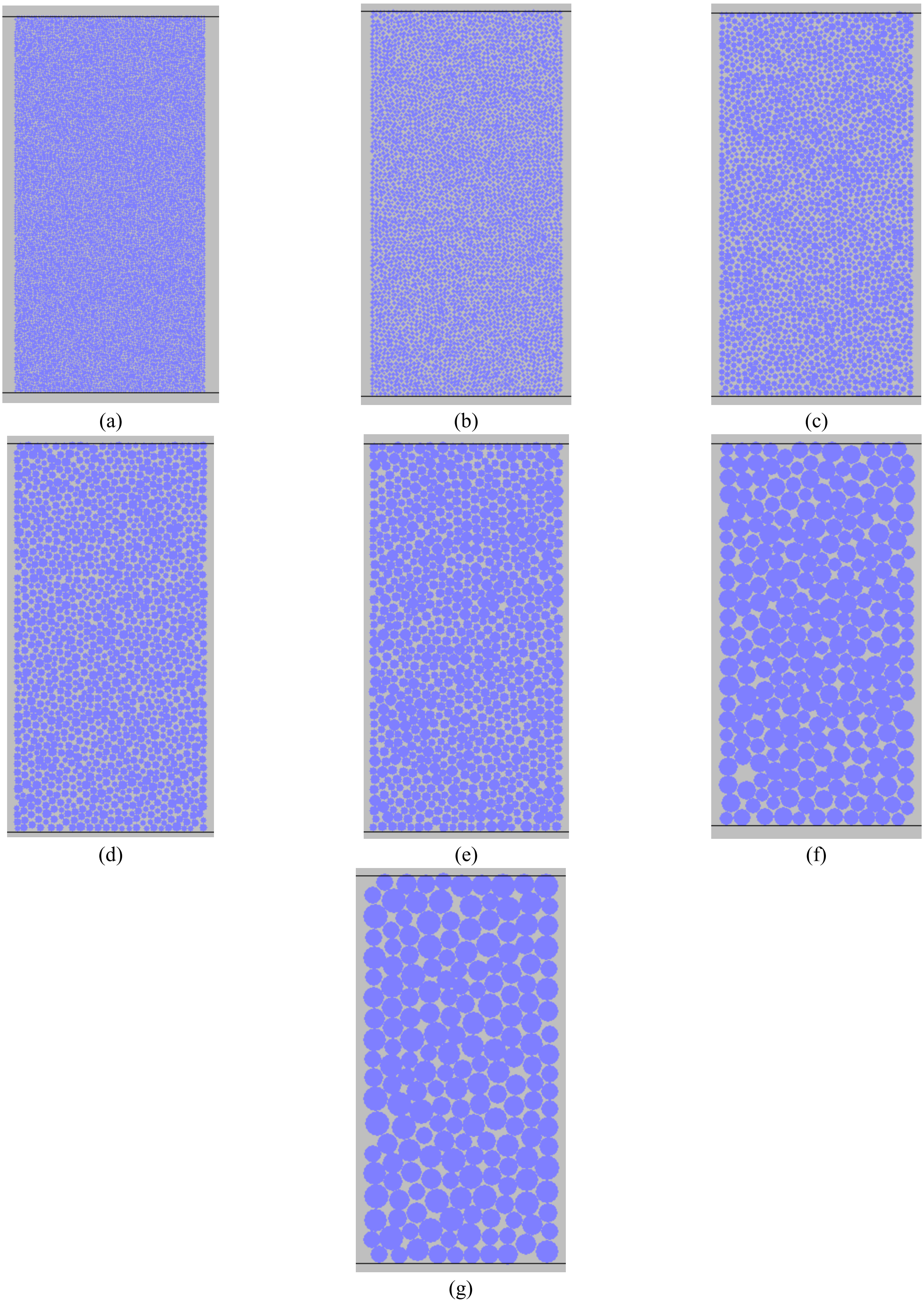

Fig. 2 Rectangular models with same dimension of 54 mm×108 mm and mean particle diameter of (a) 0.27 mm, (b) 0.47 mm, (c) 0.67 mm, (d) 0.87 mm, (e) 1.07 mm, (f) 1.87 mm and (g) 2.27

of three different models in PFC2D. Adopting the micro-properties listed in Table 1 with the standard calibration procedures (Potyondy and Cundall 2004), three calibrated PFC particle assembly was created. The diameter of the Brazilian disk considered in the numerical tests was 54 mm. The specimens were made of 5,615 particles with different

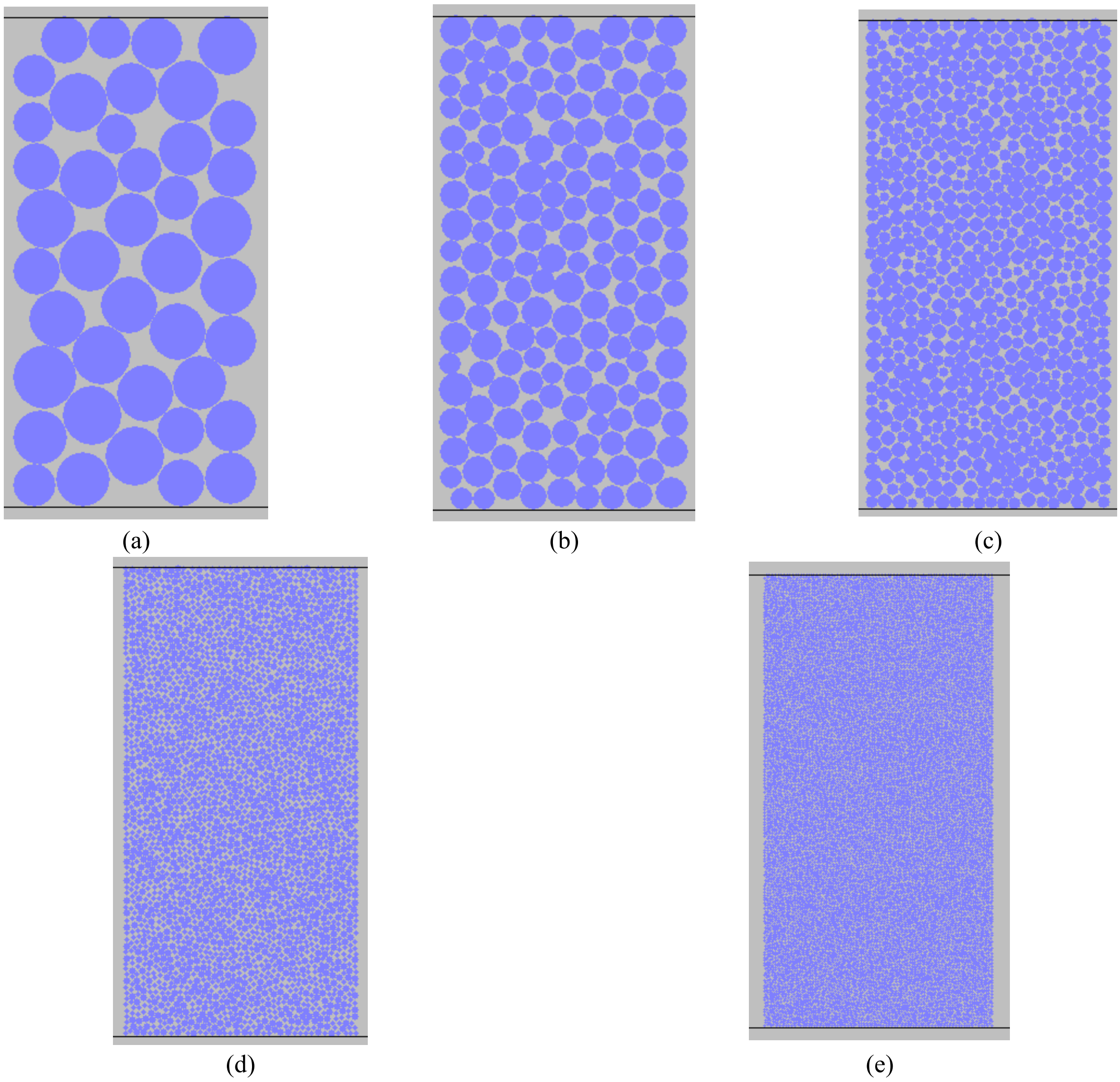

Fig. 3 Rectangular models with same mean particle diameter (0.27 mm) and dimension of (a) 3 mm×6 mm, (b) 6 mm×12 mm, (c) 12 mm×24 mm, (d) 25 mm×50 mm and (e) 54 mm×108 mm

Table 2 Brazilian tensile strength of physical and numerical samples

Physical tensile strength (MPa)	3.2
Numerical tensile strength (MPa)	3.6

clump particle distributed in it to gain the best results. The disk was crushed by the lateral walls moved toward each other with a low speed of 0.016 m/s. Fig. 1(a), (b) illustrate the failure pattern of the numerical and experimental tested samples, respectively. The failure planes experienced in numerical and laboratory tests are well matching. The numerical tensile strength and a comparison of its experimental measurements are presented in Table 2. Also Fig. 1(c) shows numerical tensile strength and a comparison of its experimental measurements. Table 2 and Fig. 1(c) show a good accordance between numerical and experimental results.

3.2 Numerical simulation

3.2.1 Preparing the model

After calibration of PFC2D, uniaxial compressive test was simulated by creating rectangular models (Fig. 2). Seven models with similar dimension of 54 mm×108 mm, and different particle size of 0.27 mm, 0.47 mm, 0.67 mm, 0.87 mm, 1.07 mm, 1.87 mm and 2.27 mm were prepared (Fig 2). Also, five rectangular models with similar particle sizes, 0.27 mm, and dimension of 3 mm×6 mm, 6 mm×12 mm, 12 mm×24 mm, 25 mm×50 mm and 54 mm×108 mm, were prepared (Fig. 3). Two loading wall were situated in the top and bottom of the models. Lower wall moves in Y direction and upper wall moves in opposite side of Y direction with a low speed of 0.016 m/s. concurrent with uniaxial test, direct shear test was performed on four numerical models. Dimension of the models were 75×100 mm. Two narrow bands of particles with dimension of 37.5 mm × 20 mm were removed from upper and lower of the model to supply the shear test condition (Fig. 4). The particle sizes change in four different values of 0.47 mm,

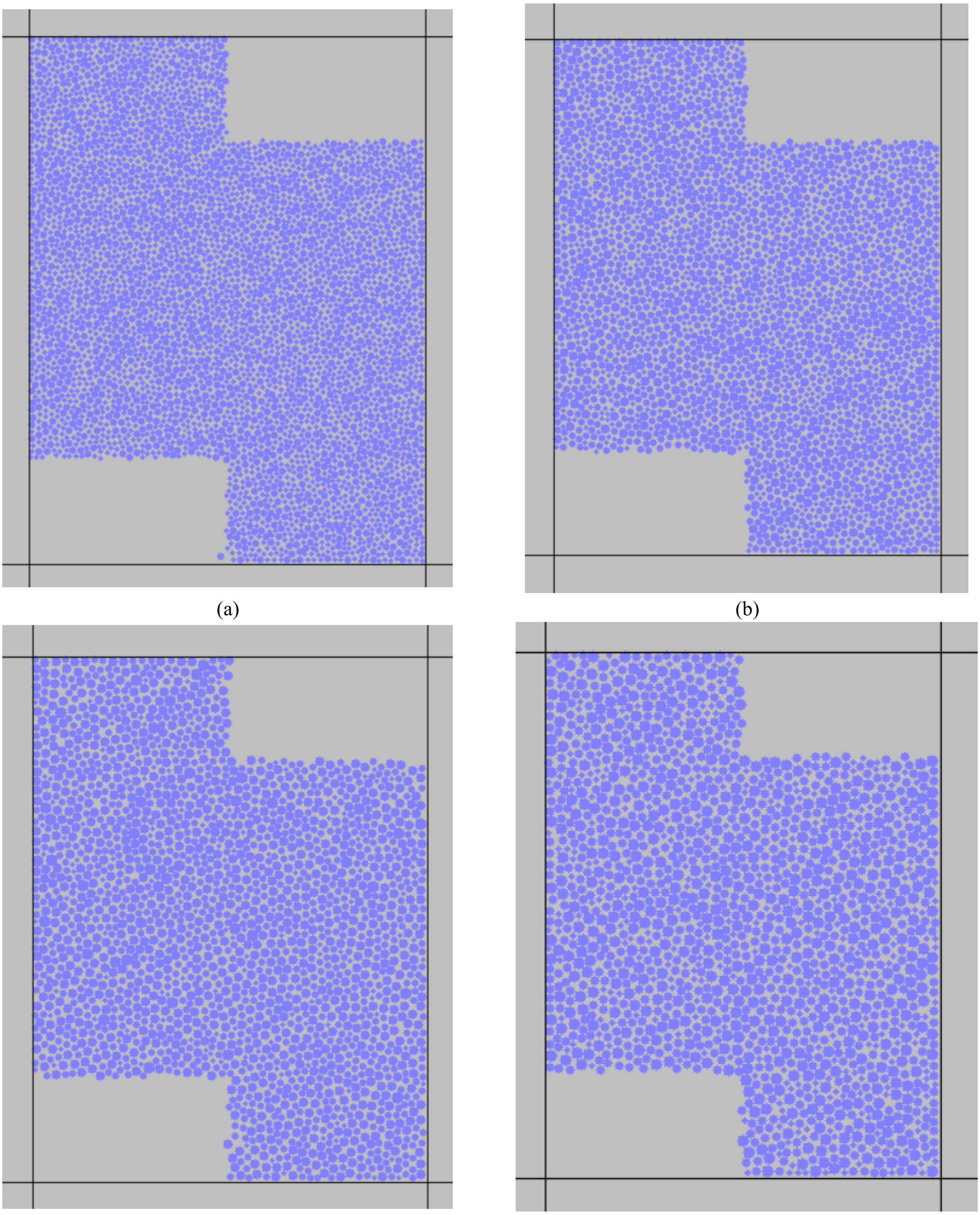

(a) (b) (c) (d)

Fig. 4 Rectangular models with same dimension of 75 mm×100 mm and mean particle diameter of (a) 0.47 mm, (b) 0.57 mm, (c) 0.67 mm and (d) 0.77 mm

0.57 mm, 0.67 mm and 0.77 mm (Fig. 4(a), (b), (c) and (d). Lower wall moves in Y direction and upper wall moves in opposite side of Y direction with a low speed of 0.016 m/s. The models are under normal stress of 8 MPa. Left wall moves in X direction till desired normal stress was reached.

3.2.2 Failure mechanism of numerical models

a) Effect of mean particle diameter on the failure pattern

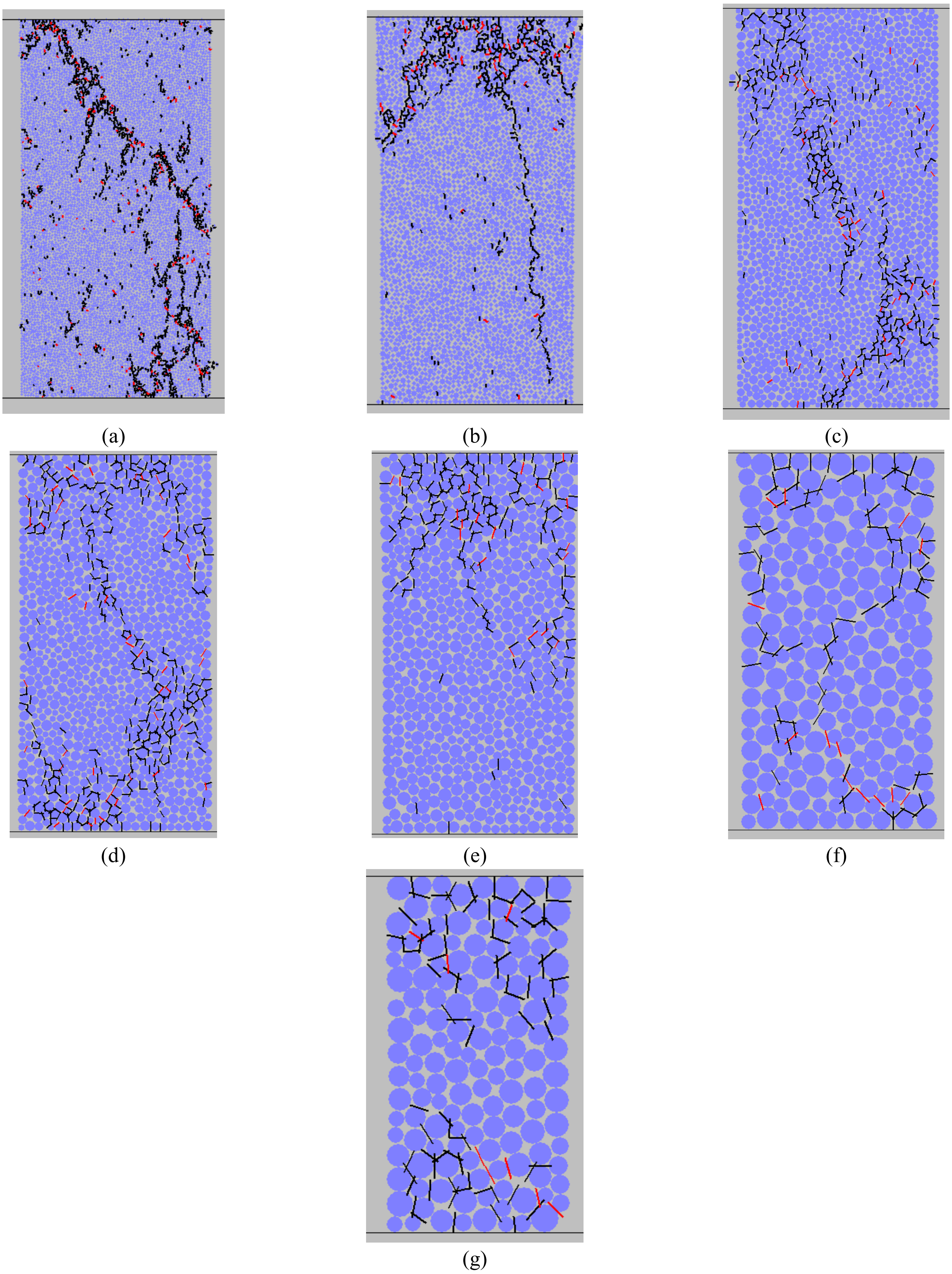

Fig. 5 Failure pattern in semicircular models with mean particle diameter of (a) 0.27 mm, (b) 0.47mm, (c) 0.67 mm, (d) 0.87 mm, (e) 1.07 mm and (f) 1.27 mm; diameter of all models is 54mm

in UCS test

Fig. 5(a)-(g) shows progress of cracks in the rectangular models with mean particle size of 0.27 mm, 0.47 mm, 0.67 mm, 0.87 mm, 1.07 mm, 1.87 mm and 2.27, respectively. Black line and red line represent tensile cracks and shear cracks, respectively. It's clear that tensile cracks are dominant mode of failure occurs in all models. The cracks propagate in a diagonal path when mean particle sizes are small. The cracks were distributed at top and bottom of the model with increasing the particle size.

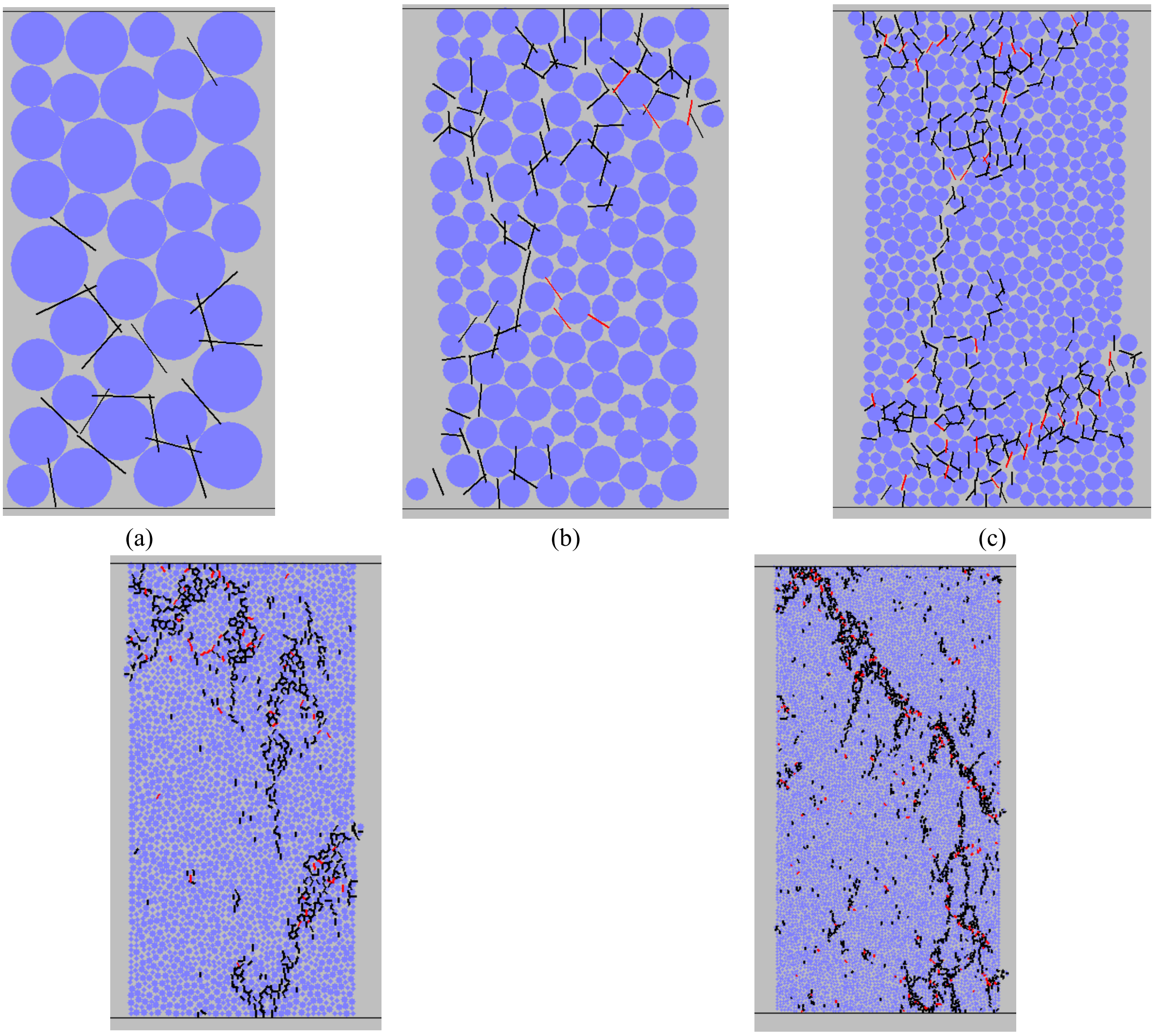

(a) (b) (c) (d) (e)

Fig. 6 Failure pattern in semicircular models with diameter of (a) 75 mm, (b) 54 mm, (c) 25 mm, (d) 12.5 mm; particle diameter in all models is 0.27 mm

b) Effect of model dimension on the failure pattern in UCS test

Fig. 6(a)-(e) shows progress of cracks in rectangular models with dimension of 3 mm×6 mm, 6 mm×12 mm, 12 mm×24 mm, 25 mm×50 mm and 54 mm×108 mm, respectively. Black line and red line represent tensile cracks and shear cracks, respectively. It's clear that tensile cracks are dominant mode of failure occurs in all models. The failure pattern is nearly constant in all models. In other word, in constant particle size, model dimension has not any effect on the failure pattern.

c) Effect of mean particle diameter on the failure pattern in direct shear test

Fig. 7(a)-(d) shows progress of cracks in the rectangular models with mean particle size of 0.47 mm, 0.57 mm, 0.67 mm and 0.77 mm, respectively. Black line and red line represent tensile cracks and shear cracks, respectively. It's clear that tensile cracks are dominant mode of failure occurs in all models. The shear bands propagate in all models. The lengths of oriented cracks were increases with increasing the particle size.

3.2.3 The effect of model scale and uniaxial compressive strength

Fig. 8 shows the effect of model diameter on the UCS while the particle size is constant.

In constant particle size, The UCS increases with increasing the diameter of the models.

3.2.4 The effect of particle size on Brazilian tensile strength

Fig. 9 shows the effect of particle size on the UCS while model scale is constant (54×108). In constant model scale, UCS increases with increasing the diameter of particles.

3.2.5 The effect of particle size on the shear strength

Fig. 10 shows the effect of particle size on the shear strength while model scale is constant (75×100). In constant model scale, shear strength increases with increasing the diameter of particles.

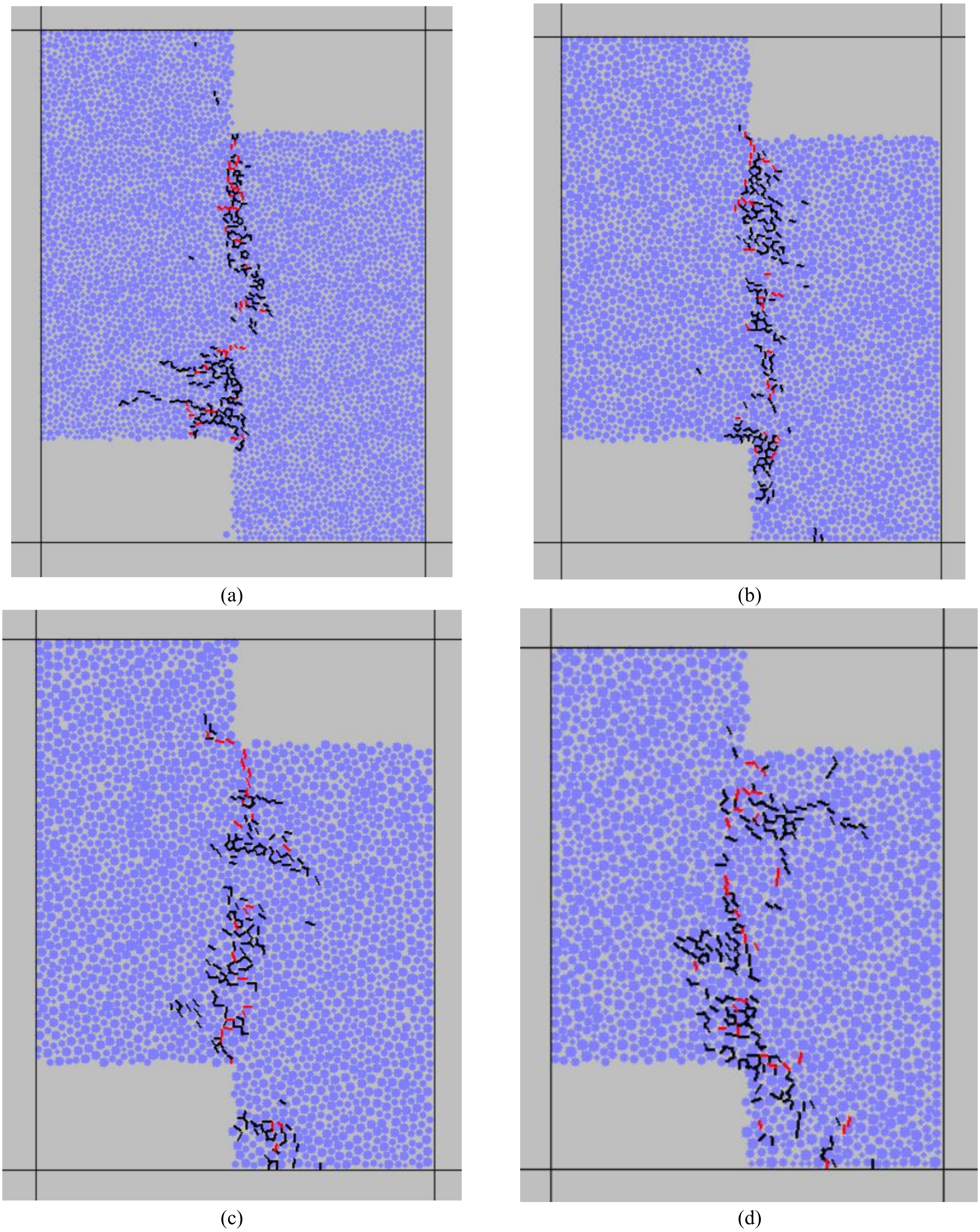

(a) (b) (c) (d)

Fig. 7 Failure pattern in models with mean particle diameter of (a) 0.47 mm, (b) 0.57 mm, (c) 0.67 mm, (d) 0.77 mm; diameter of all models is 54 mm

4. Results

This paper investigates the effects of model scale and particle size on the uniaxial compressive strength and failure processes of PFC2D numerical models. For this purpose, rectangular models with same particle size, 0.27 mm, and different model dimension, 3 mm×6 mm, 6 mm×12 mm, 12 mm×24 mm, 25 mm×50 mm and 54 mm×108 mm, were prepared. Also rectangular model with

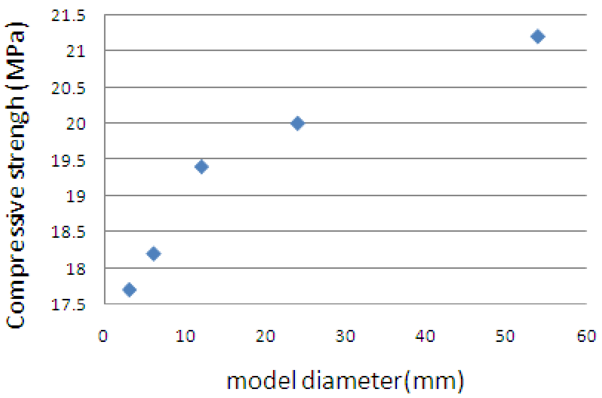

Fig. 8 the effect of model diameter on the compressive strength

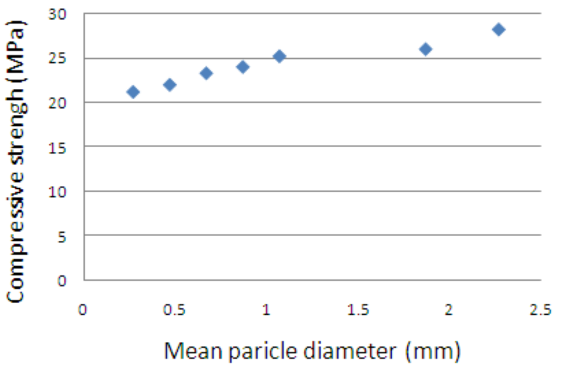

Fig. 9 the effect of particle size on the uniaxial compressive strength

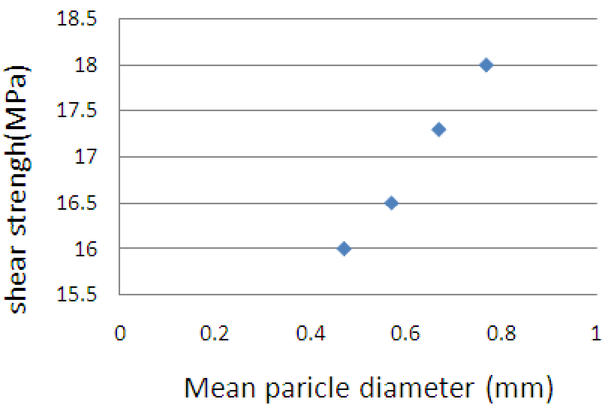

Fig. 10 the effect of particle size on the shear strength

diameter of 54 mm and different particle sizes, i.e., 0.27 mm, 0.47 mm, 0.67 mm, 0.87 mm, 1.07 mm, 1.87 and 2.27 mm were simulated using PFC2D and tested under UCS test. The result shows that tensile cracks are dominant mode of failure occur in all models. The cracks propagate in a diagonal path when mean particle sizes are small. The cracks were distributed at top and bottom of the model with increasing the particle size.

Also, failure pattern is constant by increasing the model scale. The compressive strength was increased by increasing the model diameter and particle size.

In direct shear test, the shear bands propagate in all models. The lengths of oriented cracks were increases with increasing the particle size. Also the shear strength was increased by increasing the particle size.

References

Al-Busaidi, A., Hazzard, J.F. and Young, R.P. (2005), “Distinct element modeling of hydraulically fractured lac du Bonnet granite”, *J. Geophys. Res.*, **110**(B6), B06302.

Aoki, K., Mito, Y., Mori, T., Morioka, H. and Maejima. (2004), “Evaluation of behavior of EDZ around rock cavern by AE measurement and DEM Simulation using bonded particle model”, 327-333.

ASTM (2002), “Standard test method for determination of the point load strength index of rock”, *Am. Soc. Test Mater.*, ASTM D 5731-02.

Bahaaddini, M., Hagan, P.C., Mitra, R. and Hebblewhite, B.K. (2014), “Parametric study of smooth joint parameters on the shear behaviour of rock joints”, *Rock Mech. Rock Eng.*, **48**(3), 923-940.

Bahaaddini, M., Sharrock, G. and Hebblewhite, B.K. (2013a), “Numerical direct shear tests to model the shear behaviour of rock joints”, *Comput. Geotech.*, **51**, 101-115.

Bahaaddini, M., Sharrock, G. and Hebblewhite, B.K. (2013b), “Numerical investigation of the effect of joint geometrical parameters on the mechanical properties of a non-persistent jointed rock mass under uniaxial compression”, *Comput. Geotech.*, **49**, 206-225.

Burbidge, D.R. and Braun, J. (2002), “Numerical models of the evolution of accretionary wedges and fold-and-thrust belts using the distinct-element method”, *Geophys. J. Int.*, **148**(3), 542-561.

Chiu, C.C., Wang, T.T., Weng, M.C. and Huang, T.H. (2013), “Modeling the anisotropic behavior of jointed rock mass using a modified smooth-joint model”, *Int. J. Rock Mech. Min. Sci.*, **62**, 14-22.

Cundall, P.A. (1971), “A computer model for simulating progressive large scale movements in blocky rock systems”, *Proceedings of the Symposium of the International Society for Rock Mechanics*, Nancy, France.

Cundall, P.A. (2001), *Numerical Experiments on Rough Joints in Shear Using a Bonded Particle Model*, In: Lehner, F.K., Urai, J.L., Editors, Aspects of tectonic faulting (Festschrift in Honour of George Mandl), Springer, Berlin, Germany.

Cundall, P.A. (2011), “The synthetic rock mass approach for jointed rock mass modeling”, *Int. J. Rock Mech. Min. Sci.*, **48**(2), 219-244.

Cundall, P.A. and Strack, O.D.L. (1979), “A discrete numerical model for granular assemblies”, *Geotech.*, **29**(1), 47-65.

Dalguer, L.A., Ikikura, K. and Riera, J.D. (2003), “Generation of new cracks accompanied by the dynamic shear rupture propagation of the 2000 Tottori (Japan) earthquake”, *Bull Seismol. Soc. Am.*, **93**(5), 2236-2252

Diederichs, M.S., Kaiser, P.K. and Eberhardt, E. (2004), “Damage initiation and propagation in hard rock during tunneling and the influ-ence of near-face stress rotation”, *Int. J. Rock Mech. Min. Sci.*, **41**(5), 785-812.

Erickson, S.G., Strayer, L.M. and Suppe, J. (2001), “Initiation and reactiva-tion of faults during movement over a thrust-fault ramp: Numerical mechanical models”, *J. Struct. Geol.*, **23**(1), 11-23.

Esmaieli, K., Hadjigeorgiou, J. and Grenon, M. (2010), “Estimating geometrical and mechanical REV based on synthetic rock mass models at Brunswick mine”, *Int. J. Rock Mech. Min. Sci.*, **47**(6), 915-926.

Fakhimi, A., Carvalho, F., Ishida, T. and Labuz, J.F. (2002), "Simulation of failure around a circular opening in rock", *Int. J. Rock Mech. Min. Sci.*, **39**(4), 507-515.

Fan, X., Kulatilake, P.H.S.W. and Chen, X. (2015), "Mechanical behavior of rock-like jointed blocks with multi-non-persistent joints under uniaxial loading: A particle mechanics approach", *Eng. Geol.*, **190**, 17-32.

Fan, Y., Zhu, Z., Kang, J. and Fu, Y. (2016), "The mutual effects between two unequal collinear cracks under compression", *Math. Mech. Sol.*, **22**(5), 1205-1218.

Ghazvinian, A., Sarfarazi, V., Schubert, W. and Blumel, M. (2012), "A study of the failure mechanism of planar non-persistent open joints using PFC2D", *Rock Mech. Rock Eng.*, **45**(5), 677-693.

Hadjigeorgiou, J., Esmaieli, K. and Grenon, M. (2009), "Stability analysis of vertical excavations in hard rock by integrating a fracture system into a PFC model", *Tunn. Undergr. Sp. Technol.*, **24**(3), 296-330.

Haeri, H. (2015), "Influence of the inclined edge notches on the shear-fracture behavior in edge-notched beam specimens", *Comput. Concrete*, **16**(4), 605-623.

Haeri, H. (2015), "Simulating the crack propagation mechanism of pre-cracked concrete specimens under shear loading conditions", *Strength Mater.*, **47**(4), 618-632.

Haeri, H. and Sarfarazi, V. (2016a), "The effect of micro pore on the characteristics of crack tip plastic zone in concrete", *Comput. Concrete*, **17**(1), 107-112.

Haeri, H. and Sarfarazi, V. (2016b), "The effect of non-persistent joints on sliding direction of rock slopes, computers and concrete", **17**(6), 723-737.

Haeri, H., Khaloo, A. and Marji, M.F. (2014), "A coupled experimental and numerical simulation of rock slope joints behavior", *Arab. J. Geosci.*, **8**(9), 729-7308.

Haeri, H., Khaloo, A. and Marji, M.F. (2015a), "Experimental and numerical simulation of the microcrack coalescence mechanism in rock-like materials", *Strength Mater.*, **47**(5), 740-754.

Haeri, H., Khaloo, A. and Marji, M.F. (2015b), "Fracture analyses of different pre-holed concrete specimens under compression", *Acta Mech. Sin.*, **31**(6), 855-870.

Haeri, H., Sarfarazi, V. and Hedayat, A. (2016), "Suggesting a new testing device for determination of tensile strength of concrete", *Struct. Eng. Mech.*, **60**(6), 939-952.

Haeri, H., Sarfarazi, V. and Khaloo, A. (2016), "Experimental study of shear behavior of planar non- persistent joint", *Comput. Concrete*, **17**(5), 639-653.

Haeri, H., Sarfarazi, V. and Lazemi, H.A. (2016), "Experimental study of shear behavior of planar non-persistent joint", *Comput. Concrete*, **17**(5), 639-653.

Haeri, H., Shahriar, K., Marji, M.F. and Moarefvand, P. (2013), "Modeling the propagation mechanism of two random micro cracks in rock samples under uniform tensile loading", *Proceedings of the 13th International Conference on Fracture*, Beijing, China, June.

Hazzard, J.F. and Young, R.P. (2000), "Simulating acoustic emissions in bonded-particle models of rock", *Int. J. Rock Mech. Min. Sci.*, **37**(5), 867-872.

Hazzard, J.F. and Young, R.P. (2004), "Dynamic modelling of induced seismicity", *Int. J. Rock Mech. Min. Sci.*, **41**(8), 1365-1376.

Holt, R.M., Doornhof, D. and Kenter, C.J. (2003), "Use of discrete particle modeling to understand stress-release effects on mechanical and petrophysical behavior of granular rocks", *Proceedings of the 1st International PFC Symposium*, Gelsenkirchen, Germany.

ISRM (1978), "International society for rock mechanics, commission on standardization of laboratory and field tests. Suggested methods for determining tensile strength of rock materials", *Int. J. Rock Mech. Min. Sci. Geomech. Abstr.*, **15**, 99-103.

Itasca (1999), *PFC2D-Particle Flow Code in 2 Dimensions. Theory and Background*, Itasca Consulting Group, Minneapolis, U.S.A.

Kim, J. and Taha, M.R. (2014), "Experimental and numerical evaluation of direct tension test for cylindrical concrete specimens", *Adv. Civil Eng.*, 1-8.

Konietzky, H. *Numerical Modeling in Micromechanics via Particle Methods*, Swets & Zeitlinger, Lisse, the Netherlands.

Lambert, C. and Coll, C. (2014), "Discrete modeling of rock joints with a smooth-joint contact model", *J. Rock Mech. Geotech. Eng.*, **6**(1), 1-12.

Lancaster, I.M., Khalid, H.A. and Kougioumtzoglou, I.A. (2013), "Extended FEM modelling of crack propagation using the semi-circular bending test", *Constr. Build. Mater.*, **48**, 270-277.

Li, S., Wang, H., Li, Y., Li, Q., Zhang, B. and Zhu, H. (2016), "A new mini-grating absolute displacement measuring system for static and dynamic geomechanical model tests", *Measure.*, **82**, 421-431.

Liu, X., Nie, Z., Wu, S. and Wang, C. (2015), "Self-monitoring application of conductive asphalt concrete under indirect tensile deformation", *Case Stud. Constr. Mater.*, **3**, 70-77.

Mas Ivars, D., Pierce, M.E., Darcel, C., Reyes-Montes, J., Potyondy, D.O., Paul Young, R., Mobasher, B., Bakhshi, M. and Barsby, C. (2014), "Backcalculation of residual tensile strength of regular and high performance fibre reinforced concrete from flexural tests", *Constr. Build. Mater.*, **70**, 243-253.

Mora, P. and Place, D. (1993), "A lattice solid model for the nonlinear dynamics of earthquakes", *Int. J. Mod. Phys.*, **4**(6), 1059-1074.

Mora, P. and Place, D. (1998), "Numerical simulation of earthquake faults with gouge: Toward a comprehensive explanation for the heat flow paradox", *J. Geophys. Res.*, **103**(B9), 21067-21089.

Morgan, J.K. and Boettcher, M.S. (1999), "Numerical simulations of granular shear zones using the distinct element method-1. Shear zone kinematics and the micromechanics of localization", *J. Geophys. Res.*, **104**(B2), 2703-2719.

Noel, M. and Soudki, K. (2014), "Estimation of the crack width and deformation of FRP reinforced concrete flexural members with and without transverse shear reinforcement", *Eng. Struct.*, **59**, 393-398.

Ohnishi, Y. and Aoki, K. (2004), "Contribution of rock mechanics to the new century", *Proceedings of the 3rd Asian Rock Mechanics Symposium*, Mill Press, Rotterdam, the Netherlands.

Okabe, T., Haba, T., Mitarashi, Y., Tezuka, H. and Jiang, Y. (2004), "Study on the effect of tunnel face stabilization using the distinct element method", *Proceedings of the 3rd Asian Rock Mechanics Symposium*, Mill Press, Rotterdam, the Netherlands.

Oliveira, H.L. and Leonel, E.D. (2014), "An alternative BEM formulation, based on dipoles of stresses and tangent operator technique, applied to cohesive crack growth modeling", *Eng. Analy. Bound. Elem.*, **41**, 74-82.

Park, E.S., Martin, C.D. and Christiansson, R. (2004), "Simulation of the mechanical behavior of discontinuous rock masses using a bonded-particle model", *Proceedings of the 6th North America Rock Mechanics Symposium (NARMS)*, Houston, Texas, U.S.A.

Sainsbury, D.P., Cai, Y. and Hebblewhite, B.K. (2003), *Numerical Investigation of Crown Pillar Recovery Beneath Stabilized Rockfill*, In: Konietzky H (ed) Numerical Modeling in Micromechanics via Particle Methods, Swets & Zeitlinger, Lisse, the Netherlands.

Sardemir, M. (2016), "Empirical modeling of flexural and splitting tensile strengths of concrete containing fly ash by GEP", *Comput. Concrete*, **17**(4), 489-498.

Sarfarazi, V., Faridi, H.R., Haeri, H. and Schubert, W. (2016c), "A new approach for measurement of anisotropic tensile strength of concrete", *Adv. Concrete Constr.*, **3**(4), 269-284.

Sarfarazi, V., Haeri, H. and Bagher Shemirani, A. (2017a), "Direct and indirect methods for determination of mode I fracture toughness using PFC2D", *Comput. Concrete*, **20**(1), 39-47.

Sarfarazi, V., Haeri, H. and Khaloo, A. (2016), "The effect of non-persistent joints on sliding direction if rock slopes", *Comput. Concrete*, **17**(6), 723-737.

Sarfarazi, V., Haeri, H., Bagher Shemirani, A. and Zhu, Z. (2017b), "The effect of compression load and rock bridge geometry on the shear mechanism of weak plane", *Geomech. Eng.*, **13**(3), 57-63.

Sarfarazi, V., Haeri, H., Bagher Shemirani, A., Hedayat, A. and Hosseini, S. (2017c), "Investigation of ratio of TBM disc spacing to penetration depth in rocks with different tensile strengths using PFC2D", *Comput. Concrete*, **20**(4), 429-437.

Scholtès, L. and Donzé, F.V. (2012), "Modelling progressive failure in fractured rock masses using a 3D discrete element method", *Int. J. Rock Mech. Min. Sci.*, **52**, 18-30.

Scott, D.R. (1996), "Seismicity and stress rotation in a granular model of the brittle crust", *Nat.*, **381**(6583), 592-595.

Seyferth, M. and Henk, A. (2002), "Coupled DEM and FEM models: An approach to bridge the gap between large-scale geodynamic and high-resolution tectonic modeling", *EOS Trans.* (*Fall Meet. Suppl*)., **83**, 1376-1377.

Seyferth, M. and Henk, A. (2006), "A numerical sandbox: High-resolution distinct element models of halfgraben formation", *Int. J. Earth Sci.*, **95**(2), 189-203.

Shaowei, H., Aiqing, X., Xin, H. and Yangyang, Y. (2016), "Study on fracture characteristics of reinforced concrete wedge splitting tests", *Comput. Concrete*, **18**(3), 337-354.

Shuraim, A.B., Aslam, F., Hussain, R. and Alhozaimy, A. (2016), "Analysis of punching shear in high strength RC panels-experiments, comparison with codes and FEM results", *Comput. Concrete*, **17**(6), 739-760.

Silva, R.V., Brito, J. and Dhir, R.K. (2015), "Tensile strength behaviour of recycled aggregate concrete", *Constr. Build. Mater.*, **83**, 108-118.

Strayer, L.M. and Suppe, J. (2002), "Out-of-plane motion of a thrust sheet during along-strike propagation of a thrust ramp: A distinct-element approach", *J. Struct. Geol.*, **24**(4), 637-650.

Tannant, D.D. and Wang, C. (2004), "Thin tunnel liners modeled with particle flow code", *Eng. Comput.*, **21**(2/3/4), 318-342.

Tiang, Y., Shi, S., Jia, K. and Hu, S. (2015), "Mechanical and dynamic properties of high strength concrete modified with lightweight aggregates presaturated polymer emulsion", *Constr. Build. Mater.*, **93**, 1151-1156.

Van Vliet, M.R.A. and Van Mier, J.G.M. (2000), "Experimental investigation of size effect in concrete and sandstone under uniaxial tension", *Eng. Fract. Mech.*, **65**(2-3), 165-188.

Vietor, T. (2003), "Numerical simulation of collisional orogeny using the distinct element technique", In: Konietzky, H. (ed) Numerical Modeling in Micromechanics via Particle Methods, Swets& Zeitlinger, Lisse, the Netherlands.

Vorechovsky, M. (2007), "Interplay of size effects in concrete specimens under tension studied via computational stochastic fracture mechanics", *Int. J. Sol. Struct.*, **44**(9), 2715-2731.

Wan Ibrahim, M.H., Hamzah, A.F., Jamaluddin, N., Ramadhansyah, P.J. and Fadzil, A.M. (2015), "Split tensile strength on self-compacting concrete containing coal bottom ash", *Proc.-Soc. Behav. Sci.*, **198**, 2280-2289.

Wang, C., Tannant, D.D. and Lilly, P.A. (2003), "Numerical analysis of the stability of heavily jointed rock slopes using PFC2D", *Int. J. Rock Mech. Min. Sci.*, **40**(3), 415-424

Wang, Y., Zhou, X.P. and Kou, M. (2018a), "A coupled thermo-mechanical bond-based peridynamics for simulating thermal cracking in rocks", *Int. J. Fract.*, **211**(19).

Wang, Y., Zhou, X.P. and Kou, M. (2018b), "Peridynamic investigation on thermal fracturing behavior of ceramic nuclear fuel pellets under power cycles", *Ceram. Int.*, **44**(10), 11512-11542.

Wang, Y., Zhou, X.P., Wang, Y. and Shou, Y. (2018), "A 3-D conjugated bond-pair-based peridynamic formulation for initiation and propagation of cracks in brittle solids", *Int. J. Sol. Struct.*, **134**, 89-115.

Wang, Y.T., Zhou, X.P. and Shou, Y.D. (2017), "The modeling of crack propagation and coalescence in rocks under uniaxial compression using the novel conjugated bond-based peridynamics", *Int. J. Mech. Sci.*, **128**, 614-643.

Wang, Y.T., Zhou, X.P. and Xu, X. (2016), "Numerical simulation of propagation and coalescence of flaws in rock materials under compressive loads using the extended non-ordinary state-based peridynamics", *Eng. Fract. Mech.*, **163**, 248-273.

Zhou, X.P. (2010), "Dynamic damage constitutive relation of mesoscopic heterogenous brittle rock under rotation of principal stress axes", *Theoret. Appl. Fract. Mech.*, **54**(2), 110-116.

Zhou, X.P. and Bi, J. (2018), "Numerical simulation of thermal cracking in rocks based on general particle dynamics", *J. Eng. Mech.*, **144**(1), 04017156.

Zhou, X.P. and Wang, Y. (2016), "Numerical simulation of crack propagation and coalescence in pre-cracked rock-like Brazilian disks using the non-ordinary state-based peridynamics", *Int. J. Rock Mech. Min. Sci.*, **89**, 235-249.

Zhou, X.P. and Wang, Y. (2016), "Numerical simulation of initiation, propagation and coalescence of cracks using the non-ordinary state-based peridynamics", *Int. J. Fract.*, **201**(2), 213-234.

Zhou, X.P. and Wang, Y.T. (2016), "Numerical simulation of crack propagation and coalescence in pre-cracked rock-like Brazilian disks using the non-ordinary state-based peridynamics", *Int. J. Rock Mech. Min. Sci.*, **89**, 235-249.

Zhou, X.P. and Yang, H.Q. (2007), "Micromechanical modeling of dynamic compressive responses of mesoscopic heterogenous brittle rock", *Theoret. Appl. Fract. Mech.*, **48**(1), 1-20.

Zhou, X.P. and Yang, H.Q. (2012), "Multiscale numerical modeling of propagation and coalescence of multiple cracks in rock masses", *Int. J. Rock Mech. Min. Sci.*, **55**, 15-27.

Zhou, X.P., Wang, Y., Shou, Y. and Kou, M. (2018), "A novel conjugated bond linear elastic model in bond-based peridynamics for fracture problems under dynamic loads", *Eng. Fract. Mech.*, **188**, 151-183.

Zi, G., Kim, J. and Bazant, Z.P. (2014), "Size effect on biaxial flexural strength of concrete", *ACI Mater. J.*, **111**(3), 1-8.

CC